

Self-Termination of Borophene Edges

Lu Qiu, Yüewen Mu, Sung Youb Kim,* and Feng Ding*



Cite This: *JACS Au* 2024, 4, 116–124



Read Online

ACCESS |

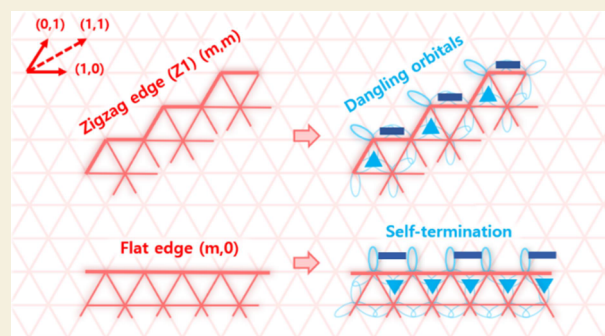
Metrics & More

Article Recommendations

Supporting Information

ABSTRACT: Due to boron's unique bonding nature, planar boron materials, including borophenes, boron nanoclusters, and nanoribbons, show very puzzling features, especially the superior stability of the free-standing planar boron edges. Here, we present a systematic investigation of the bonding configurations of various edges of borophene. Because of the flexibility of forming either three-center two-electron ($3c-2e$) or two-center two-electron bonds ($2c-2e$), an edge of borophene tends to be self-terminated by adopting a different bonding configuration at the edge from that in bulk. Among various borophene edge types, the double-chain-terminated flat edge is found to be significantly stable. As a consequence, we found that the double- and triple-chain borophene nanoribbons with a triangular lattice and wider ribbons with hexagonal holes in the central area are more stable than the quadruple-chain borophene nanoribbon. This study greatly deepens our understanding of the bonding configurations, electronic properties, and stabilities of planar boron nanostructures and paves the way for the rational design and synthesis of various boron materials.

KEYWORDS: borophene, edge, self-termination, density functional theory, chemical bond



deepens our understanding of the bonding configurations, electronic properties, and stabilities of planar boron nanostructures and paves the way for the rational design and synthesis of various boron materials.

INTRODUCTION

Since the experimental realization of all-boron fullerene¹ and theoretically predicted boron polymorphs,^{2,3} planar boron-only materials, especially various two-dimensional (2D) boron sheets, namely borophene, have recently attracted growing interest. Due to boron's electron-deficiency nature and the related chemical bonding features,^{4,5} planar boron materials exhibit many intriguing properties. Unlike many other materials, including its carbon counterpart, free-standing planar boron nanoclusters are reported highly stable and have been successfully synthesized,^{6,7} indicating that edge energies of these planar boron clusters must be considerably low. Except for boron nanoclusters, one-dimensional boron nanostructures that have two long pristine edges, such as linear and cyclic double boron rings, are also predicted as low-energy isomers.^{7–11} More interestingly, for 2D boron sheets, polymorphs with hexagonal holes or larger holes are usually energetically more favorable,^{12–14} implying the high stability of hole edges in a triangular lattice-based borophene. All of these results suggest that the edges of borophene are significantly different from that of graphene. A pristine graphene edge has an extremely high formation energy of ~ 10 eV/nm^{15,16} and introducing hetero functional groups, such as H, OH, or O, is essential to passivate the highly unstable pristine edges of graphene. In sharp contrast, the formation energy of a borophene edge can be as low as ~ 2 eV/nm.¹⁷ Such a small edge formation energy implies that the dangling orbitals of an as-cut borophene edge must be effectively self-passivated.

Zhang and co-workers have found that, on the silver substrate, some specific types of borophene edges are very stable and might be self-passivated as the interaction between the borophene edge and the substrate is very weak.¹⁷ Some theoretical studies have proposed similar chemical bonding models with peripheral two-center two-electron ($2c-2e$) and central three-center two-electron ($3c-2e$) bonds for planar boron nanoclusters, showing different bonding configurations at the edge and bulk of 2D boron materials.^{18,19} Unfortunately, an insightful understanding of the superior stability of the borophene edge or the mechanism of dangling orbital self-termination at the edge is still missing.

Here, we investigate the borophene edge based on the theory for the chemical bonding resonance in 2D boron materials.²⁰ It is found that the flat edge in the boron triangular lattice is of high stability because of the self-termination of the edge dangling orbitals by forming $2c-2e$ bonds and a subsequent edge resonance following the $3c-2e$ bond resonance in bulk. Considering the boron nanoribbons with this most stable flat edge, using density functional theory (DFT) calculation, double- and triple-chain with perfect

Received: September 20, 2023

Revised: November 3, 2023

Accepted: November 27, 2023

Published: January 2, 2024



triangular lattice are demonstrated to be the most stable ribbons, and wider ribbons can reach similar stability by creating hexagonal holes in the central area. DFT calculation and the edge resonance model also reveal that a flat borophene edge should be protected by a boron double chain. This work proves that the pristine edge of 2D borophene can be efficiently self-terminated without interacting with any functional groups, which will benefit the design and synthesis of boron-based materials or pure boron chemistry.

RESULTS AND DISCUSSION

In the planar boron triangular lattice shown in Figure 1, we define two basic vectors, $\nu_1 = (1, 0)$ and $\nu_2 = (0, 1)$, where the

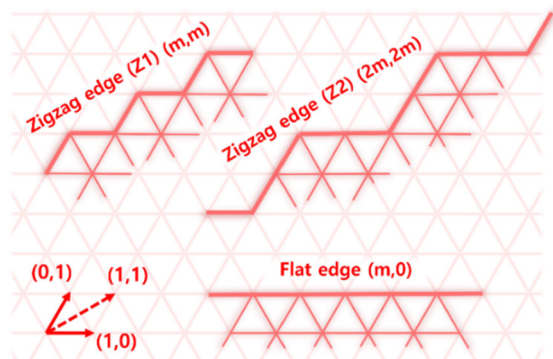


Figure 1. Schematic diagram of the borophene edges. Two types of primary borophene edges, flat (F) edges and zigzag (Z) edges, are shown in a boron triangular lattice along $(m, 0)$ and (m, m) directions, respectively. According to the oscillation amplitudes, zigzag edges can be defined as Z1, Z2, etc. as shown in the figure.

angle between the two vectors is 60 degrees. Thus, any vector connecting two lattice points can be expressed as $m\nu_1 + n\nu_2$ or (m, n) , where m and n are integers. Depending on their alignments and periodicities, borophene edges can be classified into flat edges whose indexes are $(m, 0)$, zigzag edges whose indexes are (m, m) , and chiral edges whose indexes are (m, n) ($m \neq n, n \neq 0$). Note that different oscillation amplitudes (or periodicities) along the zigzag direction lead to different edge types, such as Z1 and Z2 are different (Figure 1), and here, we denote them by (m, m) and $(2m, 2m)$, respectively. Similarly, we define zigzag edges with larger oscillation amplitudes as Z3, Z4, etc.

Self-Termination of the Edge Dangling Orbitals

In this work, following the bonding model in ref 20, we assume that all the B atoms are sp^2 hybridized (light blue orbital denotation), and in the boron triangular lattice, it tends to form either conventional $2c-2e$ (head-to-head, denoted by dark blue bar), $3c-2e$ (denoted by blue triangle) σ bonds, or a new type of shoulder-by-shoulder (π type) $2c-2e$ bonds (denoted by blue bar), as shown in Figure 2. We note that, following this bonding model, each boron atom in a highly stable borophene bulk shares six σ electrons or forms three σ bonds with its neighboring boron atoms. Together with the extra two π electrons, every boron atom in a highly stable borophene bulk fulfills the octet rule.

Using three triple-chain ribbons as examples, we consider the bonding configurations of three basic borophene edge types, Z1, Z2, and F edges (Figure 2). For the Z1 edge (Figure 2a,b), half of the triangular lattices are occupied by $3c-2e$

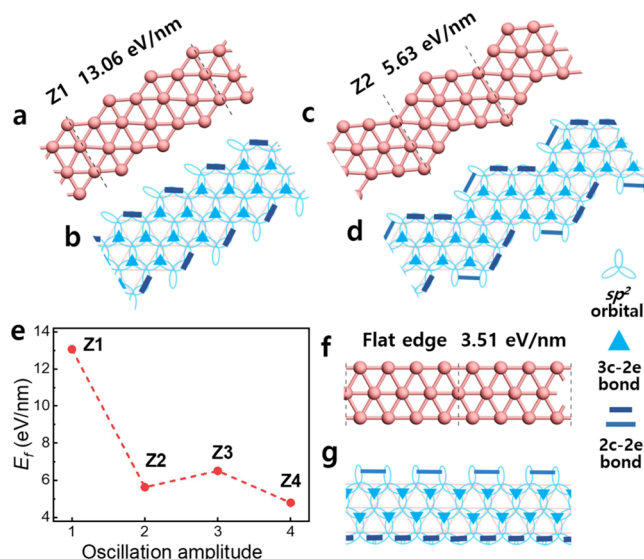


Figure 2. Chemical bonding analysis of the three basic borophene edges. (a–d) Optimized structures, formation energies, and bonding configurations of borophene ribbons with Z1 (a, b), and Z2 (c, d) edges. (e) Formation energies of various zigzag ribbons by DFT calculation. (f, g) Optimized structure, formation energy, and bonding configuration of the borophene ribbon with the flat (F) edge. The bonding analysis is performed on three triple-chain ribbons with corresponding edge types. All the B atoms are sp^2 hybridized, the borophene bulk tends to form a maximum number of $3c-2e$ bonds, and the $2c-2e$ bonds will be formed at the edge. The ribbon formation energies presented are obtained by using eq 1, and therefore, the edge energies are half of them, i.e., 6.53, 2.82, and 1.76 eV/nm, respectively.

bonds and head-to-head $2c-2e$ bonds form at half of the edge sites. The above orbital analysis shows that there is one dangling orbital at each convex corner of the Z1 edge and, thus, we predict that the Z1 edge is energetically less stable and the reconstruction of the pristine Z1 edge will occur.¹⁷

Increasing the oscillation amplitude of the zigzag edge, we have the Z2 edge (Figure 2c,d), on which half of the edges form head-to-head (σ type) $2c-2e$ bonds and another half form shoulder-by-shoulder (π type) $2c-2e$ bonds, leaving no dangling orbitals on the self-terminated Z2 edge. According to the above analysis, we predict that the Z2 edge is more stable than the Z1 edge.¹⁷

To verify the above analysis, we calculate the formation energies of a few types of ribbons, which contain the energy of two identical edges as,

$$E_f = (E_{\text{ribbon}} - N\mu_B)/L \quad (1)$$

where E_{ribbon} is the DFT calculated energy of a ribbon, N is the number of B atoms in the ribbon, μ_B is the reference energy or the energy of one B atom in a free-standing α -borophene, and L is the ribbon length. The calculation details are presented in Methods. The result shows that the energy of the Z1 edge (6.53 eV/nm) is much higher than that of the Z2 edge (2.82 eV/nm), which validates our bonding analysis of borophene ribbons shown in Figure 2. A similar analysis leads to a conclusion that all the dangling orbitals of an even-numbered zigzag edge (Z2, Z4, Z6,...) can pair up to form $2c-2e$ bonds and, in contrast, the odd-numbered zigzag edges (Z1, Z3, Z5,...) always have one unpaired dangling orbital in each periodic unit. Therefore, an oscillation of the formation

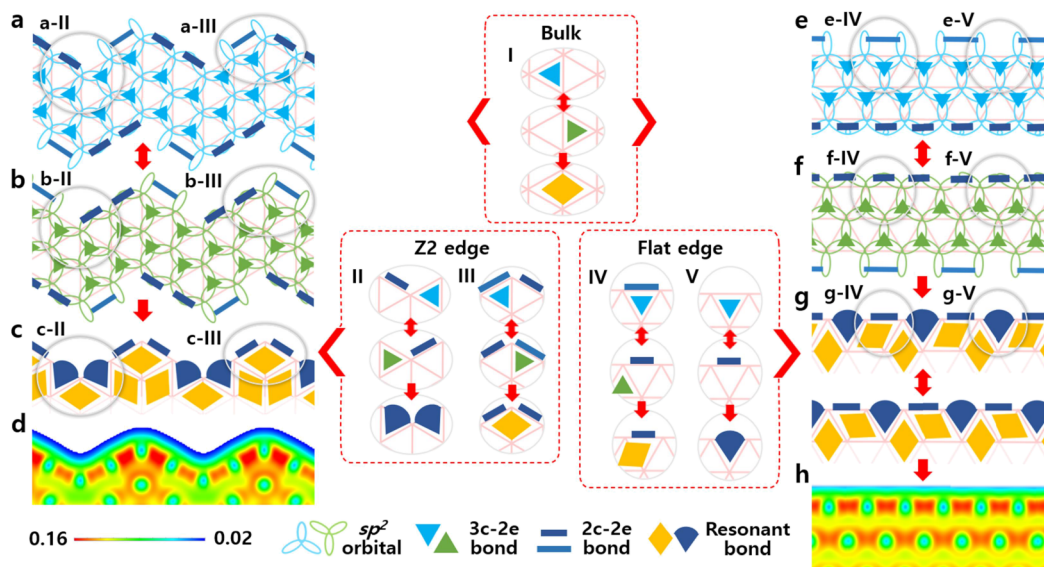


Figure 3. Resonance analysis of borophene Z2 and flat edges. (a–c) Two equivalent bonding configurations of the triple-chain borophene nanoribbon with the Z2 edges (a, b) lead to a resonant bonding structure shown in (c). (d) Corresponding valence electron charge density (VECD) map verifies the bonding analysis. (e–g) Two equivalent bonding configurations of the triple-chain borophene nanoribbon with the flat edges (e, f) lead to the resonant bonding structures shown in (g). (h) Corresponding VECD map verifies the bonding analysis of the flat borophene edge. Inset: the resonance of alternating 3c–2e bonds in the bulk of the nanoribbons (I); the resonance units involving alternating 3c–2e and 2c–2e bonds at the Z2 and flat edges (II and III; IV and V), respectively. The intensity scale bars of (d) and (h) are from 0.16 to 0.02 e/bohr³ (red to blue).

energies of zigzag ribbons is predicted. Our DFT calculation (Figures 2e and S1) also demonstrates such formation energy oscillation.

From the above DFT calculations, we can see that the formation energy of the self-terminated borophene edge is just a small fraction of that of the pristine edge of graphene,¹⁵ which implies that the pristine borophene edges can exist in ambient conditions. Among these self-terminated edges, the flat edge, whose formation energy is only 1.76 eV/nm (Figure 2f), is much more stable than the zigzag edges. To understand the stability of the flat edge, we plot the bonding configuration of a triple-chain borophene ribbon with flat edges in Figure 2g. On the bottom edge of the ribbon, head-to-head 2c–2e bonds form between each two neighboring B atoms, just like that at the hexagonal hole edge of borophene.²⁰ In contrast, in-plane shoulder-by-shoulder 2c–2e bonds form on the top edge. This indicates that all of the dangling orbitals of both edges of a flat-edged borophene ribbon are perfectly self-terminated.

We need to point out that under our current theoretical framework,²⁰ edge self-termination or no dangling orbitals at the edge is a necessary condition to ensure the high stability of the borophene nanomaterials with edges. But it is not a sufficient condition. Stabilities of borophene structures, such as borophene nanoribbons (as will be shown in the following discussion), may vary intensively even when there are no dangling orbitals and the octet rule is satisfied.

Resonance of the Borophene Edges

In the σ bond resonance theory,²⁰ energy of the flat boron system is further reduced by the resonance between the 2c–2e and 3c–2e σ bonds within the triangular lattice of the boron plane. The resonance happens between two identical bonding configurations derived from two sp^2 orbital patterns, which are denoted by the light blue and light green sp^2 orbitals shown in Figure 3. Here, the green pattern of the sp^2 orbitals can be obtained by flipping the blue pattern. In a borophene bulk (see

Figure 3a,b, or Figure 3e,f, or in the original study of ref 20, the resonance of alternating 3c–2e bonds (blue and green triangles) leads to a diamond-shaped resonant 3c–2e bond (yellow diamond), which is the type I resonance unit in Figure 3.

Following the resonance in bulk borophene, we plot another equivalent bonding configuration at the Z2 edge (Figure 3b). It is shown that the 3c–2e bonds (green) form in the other half of the triangular lattice compared to the previous blue configuration in Figure 2d (or Figure 3a), and the head-to-head and shoulder-by-shoulder 2c–2e bonds at the zigzag edges exchange their positions. The two equivalent bonding configurations thus lead to a resonant bonding structure (Figure 3c) including resonance units of (I) resonance of alternating 3c–2e bonds in the bulk results in resonant 3c–2e bonds (yellow diamond); (II) resonance of alternating 2c–2e or 3c–2e bonds at each concave corner results in two resonant 3c–2e/2c–2e bonds (dark blue sector); (III) resonance of alternating head-to-head or shoulder-by-shoulder 2c–2e bonds at each convex corner results in two mixed-type 2c–2e bonds (dark blue bar). As the electron density of a mixed-type 2c–2e bond (type III) is higher than that of a resonant 3c–2e/2c–2e bond (type II) and much higher than that of a resonant 3c–2e bond (type I), we expect higher electron density at convex corners, lower at concave corners, and lowest in the bulk, which agrees well with the valence electron charge density (VECD) map (Figure 3d). A similar resonance analysis can be applied to the Z1 edge (Figure S2).

The flat edge (Figure 3e) has another equivalent bonding configuration (Figure 3f), and the corresponding resonant bonding structures are shown in Figure 3g. In the bulk, the resonance is the same and composed of only resonance unit I. At the flat edge, there also include two resonance units of (IV) resonance of alternating head-to-head or shoulder-by-shoulder 2c–2e results in a mixed-type 2c–2e bond (dark blue bar);

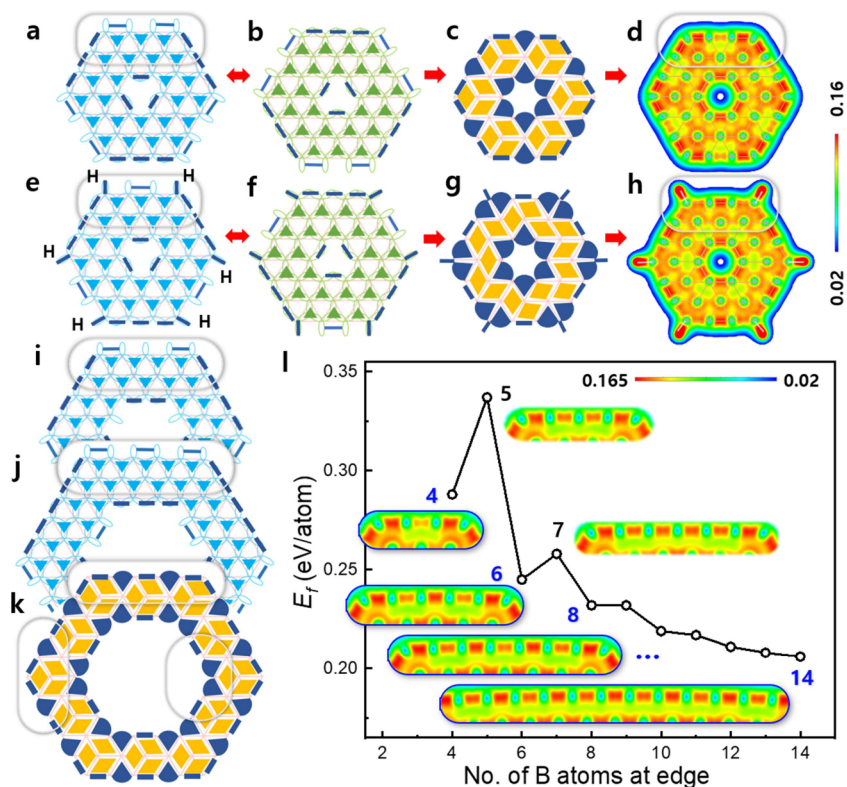


Figure 4. Bonding analysis of the flat edge using planar B_{36} nanocluster and its derivatives as examples. (a–h) Two equivalent bonding configurations, resonance bonding structures, and VECD maps of (a–d) B_{36} and (e–h) $B_{36}H_6$ nanocluster, respectively. (i, j) Bonding configurations of (i) B_{34} and (j) B_{72} nanoclusters show that there is a dangling orbital at the cluster edge with odd edge B atoms, and no dangling orbital at the cluster edge with even edge atoms. (k) Resonant bonding structure of B_{72} cluster shows the alternating $2c-2e$ and resonant $3c-2e/2c-2e$ bonds at the cluster edge. (l) Energy oscillation of the hexagonal nanoclusters with increasing size. Inserted plots are edge VECD maps of the corresponding clusters. The intensity scale bars of (d) and (h) are from 0.16 to 0.02 e/bohr^3 (red to blue), and that of (l) is from 0.165 to 0.02 e/bohr^3 (red to blue).

(V) resonance of alternating $2c-2e$ or $3c-2e$ bonds results in a resonant $3c-2e/2c-2e$ bond (dark blue sector). Therefore, the bonding configuration of the flat edge is with alternating mixed-type $2c-2e$ bonds (type IV) and resonant $3c-2e/2c-2e$ bonds (type V). The two alternating types of bonds (type IV and V), like the conjugated π bonds in graphene, can resonate again (Figure 3g, and details in Figure S3) and, therefore, lead to an evenly distributed charge density along the edge (Figures 3h and S4).

In chemistry, it is common knowledge that a stronger bond is shorter than a weak bond of the same type, such as the triple $C\equiv C$ bond is shorter than the double $C=C$ bond, and the double $C=C$ bond is shorter than the single $C-C$ bond. Since a $2c-2e$ bond is shared by two B atoms and a $3c-2e$ bond is shared by three B atoms, the bonding strength between two B atoms with a $2c-2e$ bond should be stronger than that between two B atoms with a $3c-2e$ bond, and thus, the B–B distance between two B atoms bonded with a $2c-2e$ bond should be shorter than that between two B atoms bonded with a $3c-2e$ bond. Carefully comparing the optimized B–B bond lengths at the edges of borophene nanoribbons with those in the bulk region of α -borophene (Figure S5), we find that the bond lengths match well with our bonding configuration analysis. The length of the type III $2c-2e$ bond at the vertex corner of the Z2 edge is the shortest ($\sim 7\%$ shorter than the bulk B–B bond length), that of the double-resonant bond at the flat edge is the second shortest ($\sim 5\%$ shorter than the bulk B–B bond length), that of the type II resonant $3c-2e/2c-2e$

bond is longest one at the edge (only $\sim 2.5\%$ shorter than the bulk B–B bond length), and all edge bonds are shorter than that of the bulk B–B bond length. Besides, our bonding model of the borophene edges is further validated by the solid-state adaptive natural density partitioning (SSAdNDP) analysis²¹ (Figure S6), in which $4c-2e$ bonds dominate the bulk region and $2c-2e$ or $2c-2e/3c-2e$ resonant bonds appear at the edges.

In summary, under the framework of resonance theory and our bonding model, the high stability of the borophene flat edge is attributed to the self-termination of the edge dangling orbitals and the edge resonance, which leads to the delocalized edge electronic states. Compared to the flat edge, the Z2 edge has alternating high and low electron densities along the edge,¹⁴ and therefore is less stable. Applying the same analysis, we found that the Z4 edge should be more stable than the Z2 edge. Our DFT calculation proves the analysis (Figures 2e and S1).

Verification of the Edge Bonding Configurations

The above analysis clearly shows that the resonance of bonds along an infinitely long flat edge leads to the even distribution of charge density, and thus it is impossible to identify the alternating $2c-2e$ and resonant $3c-2e/2c-2e$ bonds. We, therefore, take the well-known highly stable planar B_{36} nanocluster⁷ and its derivatives as examples to further analyze the bonding configurations of borophene edges.

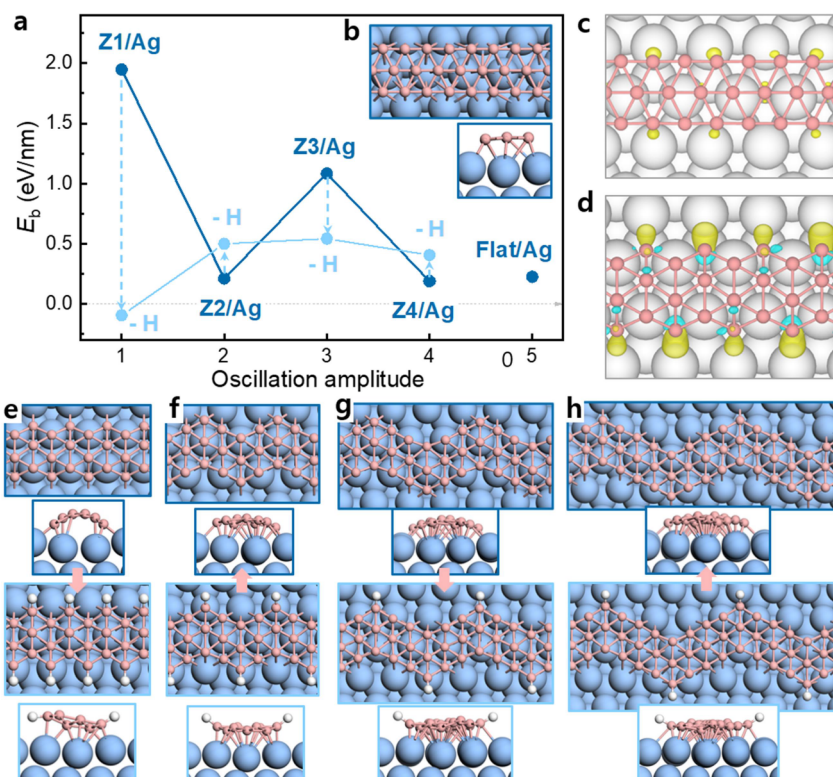


Figure 5. Interaction between borophene edges and the substrate. (a) Binding energies between borophene edges and the Ag(111) substrate. (b) Optimized structure of a triple-chain borophene nanoribbon with flat edges on the Ag(111) substrate from top and side views. (c, d) Charge density difference maps of triple-chain borophene nanoribbons with flat and Z1 edges, respectively. The isosurface level is $0.006\text{el}/\text{\AA}^3$, where yellow denotes positive charge transfer and cyan represents negative charge transfer. (e–h) Optimized structures of triple-chain borophene nanoribbons with zigzag edges (Z1, Z2, Z3, and Z4) on the Ag(111) substrate from top and side views, including their hydrogenated counterparts (shown below).

Before considering the resonance, the bonding configuration of the sp^2 hybridized B_{36} cluster has a three-fold symmetry (Figure 4a,b). Along the edge of the central hexagonal hole, there are three head-to-head $2c-2e$ σ bonds and three $3c-2e$ σ bonds. The resonance of the two equivalent bonding configurations (Figure 4a,b) leads to six resonant $3c-2e/2c-2e$ bonds along the hexagonal hole (Figure 4c), which is the same as the hexagonal hole in bulk borophene.²⁰ Along the six outer edges of the B_{36} cluster, three of them have nine total head-to-head $2c-2e$ σ bonds. On each of the left three outer edges, there are four dangling orbitals, perpendicularly pointing out. The four dangling orbitals therefore form two shoulder-by-shoulder $2c-2e$ σ bonds, similar to the extra in-plane bond that leads to the self-passivation of the graphene armchair edge (Figure S7).^{15,22} The resonance of the two equivalent bonding configurations (Figure 4a,b) therefore leads to a bonding structure as presented in Figure 4c, which perfectly matches the calculated bonding details in the literature (Figure S8).⁷ In the calculated VECD map of a planar B_{36} cluster (Figure 4d), we can easily identify the existence of the mixed-type $2c-2e$ bonds (high electron density bonds on the outer corners) and the resonant $3c-2e/2c-2e$ bonds (low electron density bonds at the center of the outer edges).

To further illustrate the bonding configuration at the edge, we compare the bonding configurations of the B_{36} cluster and its partially hydrogenated cluster, $B_{36}H_6$ (Figure 4e–h). The resonant bonding configuration of the B_{36} cluster has two mixed-type $2c-2e$ bonds at each corner (Figure 4c) and a resonant $3c-2e/2c-2e$ bond at the center of each edge, which

can be identified by the electron density distribution (Figure 4d). If we terminate the two end B atoms of an edge with hydrogen (Figure 4e,f), the two dangling σ orbitals of the two central B atoms will form a shoulder-by-shoulder $2c-2e$ σ bond. Finally, the resonant configuration along the edge has a mix-type $2c-2e$ σ bond in the center of each edge and two resonant $3c-2e/2c-2e$ σ bonds near each corner (Figure 4g). From the VECD map (Figure 4h), we can clearly see higher electron density at the center of the edge and lower electron density near each corner, which is opposite to the VECD map of B_{36} (Figure 4d). This comparison of bonding configurations of B_{36} and $B_{36}H_6$ clearly shows that the dangling orbitals at the edge can pair up by forming $2c-2e$ bonds in a way like shoulder-by-shoulder π bonds and well terminate themselves, which validates our analysis for the bonding configurations of borophene edges (see Figures S9 and S10 for more detailed analysis of the bonding configurations of B_{36} and the hydrogenated boron clusters).

The B_{36} cluster has an even number of B atoms at an edge and thus all dangling σ orbitals of the edge can be paired into $2c-2e$ bonds, which ensures that each edge of the B_{36} is dangling-orbital-free and thus highly stable. Following this analysis, we draw the bonding configurations of triple-ring-shaped boron clusters (Figure 4i–k). As shown in Figure 4i, each inner and outer edge of the B_{54} cluster has 3 and 5 boron atoms, respectively, and there are 6 unpaired σ orbitals in the bonding configuration. Therefore, we predict that the B_{54} cluster is significantly less stable than the B_{36} . Further increasing the cluster size, when the numbers of both inner

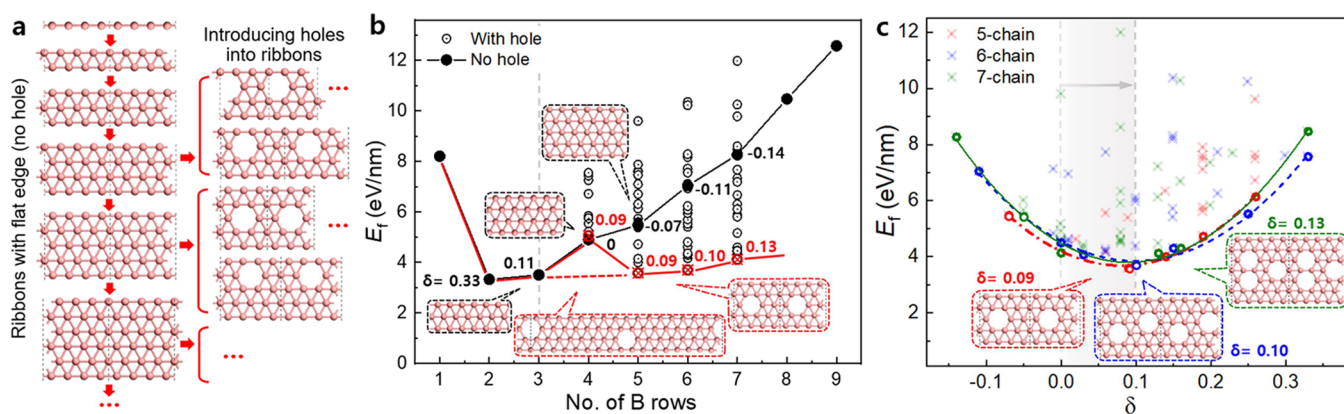


Figure 6. Stability of boron nanoribbons with flat edges. (a) Schematic diagram of ribbon structure searching. (b) Formation energies of various flat edge ribbons vs ribbon width. Black dots denote the ribbons with triangular lattice but no hexagonal hole; black circles denote the ribbons with hexagonal holes. (c) Formation energies of 5- (red), 6- (blue), and 7-chain (green) ribbons vs occupation imbalance factor $\delta = N_c^r/N_o^r - N_c^t/N_o^t$.

and outer edge B atoms are even (Figure 4j), all the edge dangling orbitals pair up, and the cluster becomes stable again. As shown in Figure 4k, alternating mixed-type $2c-2e$ (dark blue bar) bonds and resonant $3c-2e/2c-2e$ (dark blue sector) bonds appear on the flat edge.

The formation energy oscillation with an increase in the cluster size is presented in Figure 4l. When the number of edge B atoms is even, the formation energy of the cluster is greatly reduced, and the edge shows a clear alternating charge density feature (Figures 4l, S11, and S12). When the edge becomes longer enough, the energy fluctuation becomes negligible and the alternating feature of the charge density along the edge cannot be clearly seen, implying that the resonance between the mix-type $2c-2e$ bonds and $3c-2e/2c-2e$ bonds along the edge becomes dominating. Finally, delocalized bonds with evenly distributed electrons along a long edge, as presented in Figure 3h for the flat edge, are formed.

Borophene Edges on the Ag(111) Substrate

The proposed bonding configurations of the free-standing borophene edges or borophene nanoribbons have clearly shown that some edges have dangling orbitals, while some are well self-passivated. On active metal substrates, an edge with dangling orbitals tends to interact with the substrate strongly, while the well self-passivated edges interact with the substrate weakly. As an example, we calculate the binding energies between various borophene edges and the experimentally widely used Ag(111) substrate as

$$E_b = (E_{\text{ribbon}} + E_{\text{Ag}} - E_{\text{ribbon/Ag}} - N \times \varepsilon_{\text{bulk}}) / 2L \quad (2)$$

where E_{ribbon} , E_{Ag} , and $E_{\text{ribbon/Ag}}$ are the DFT calculated energies of a free-standing borophene nanoribbon, an Ag(111) metal substrate, and a borophene ribbon on the Ag substrate, respectively. N is the number of B atoms in the ribbon, $\varepsilon_{\text{bulk}}$ is the binding energy between bulk triangular borophene and the Ag(111) substrate per B atom (0.248 eV/atom), and L is the ribbon length. We note that taking the van der Waals energy between bulk borophene and the substrate as a reference to estimate that between the borophene ribbon and the substrate will lead to a slight energy deviation. However, it will not damage our main conclusion considering that the van der Waals energy deviation is very small compared to the edge binding energy. Further calculation details are presented in Methods.

The calculation results are presented in Figure 5a. It is shown that the interaction between the flat edge and the substrate is only 0.22 eV/nm or 0.035 eV per edge atom. Besides, the optimized structure of the borophene nanoribbon with flat edges on the Ag substrate shows no tendency of edge atoms bending toward the substrate (Figure 5b), and the corresponding charge density difference (CDD) map (Figure 5c) shows very limited charge transfer between the edge and the substrate. The above analysis clearly shows that the edge atoms of the flat borophene edge behave the same as the bulk atoms when interacting with the Ag(111) substrate and it is “perfectly” self-passivated.

In sharp contrast to the weak binding between the flat edge and the Ag(111) substrate, a large amount of charge transfer at each vertex corner of the Z1 edge can be seen in the CDD map (Figure 5d), and the bending of the ribbon edge toward the Ag(111) substrate is clearly shown (Figure 5e). The above analyses indicate the existence of dangling orbitals at the Z1 edges. The binding energy between the Z1 edge and the Ag(111) substrate is 1.95 eV/nm, which is about 1 order of magnitude higher than that of the flat edge (Figure 5a). To further prove this, we terminate the dangling orbitals at the vertex corners of the Z1 edge with H atoms. The binding energy of the H-terminated Z1 edge to the substrate is greatly reduced to ~ 0 , and the bending of the borophene edge is no longer observable (Figure 5a,e).

Increasing the oscillation amplitude of the zigzag nanoribbon, the binding energy between the Z2 edge and the substrate is suddenly reduced and becomes close to that between the flat edge and the substrate (Figure 5a), which can be well explained by the pairing up of the dangling orbitals and the self-termination of the Z2 edge (Figure 2d). If we terminate the Z2 edge with H atoms like those of the Z1 edge (Figure 5a,f), the binding energy between the hydrogenated Z2 edge and the substrate is increased.

The binding energies of zigzag edges with higher oscillation amplitude (or larger period) on the Ag(111) substrate (Figure 5a,g,h) show a similar odd–even oscillation (Figure 2e), which further validates our bonding analysis of the borophene edges and the effectiveness of applying it to understand the borophene edges on metal substrates. With such a simple analysis, the behavior of borophene growth on the substrates can be intuitively understood and thus could benefit the controllable synthesis of borophene.¹⁷

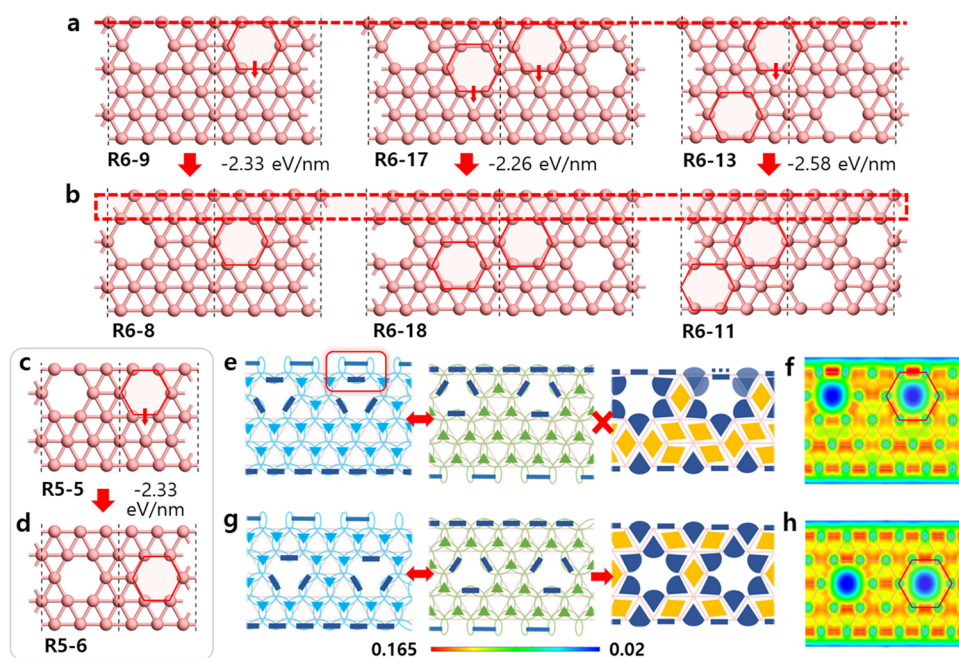


Figure 7. Double-chain protection of the borophene flat edge. (a, b) Flat-edged borophene nanoribbons with hexagonal holes at the edge (a) have higher formation energies than those with double-chain-protected ribbons (b). (c, d) Comparison between ribbons with hexagonal holes (c) at the edge and (d) at the central area, leaving the flat edge protected by the double chain. (e, f) Bonding configuration of the ribbon with holes at the edge shows the break of hole and edge resonance, which is verified by (f) the localized electron density. (g, h) Bonding configuration of the ribbon with double-chain protection shows a good resonance at both the ribbon edge and hexagonal hole edge, with the demonstration from (h) the VECD map. The intensity scale bars of (f) and (h) are from 0.165 to 0.02 e/bohr³ (red to blue).

Stability of Borophene Nanoribbons with Flat Edges

The examples presented above and the agreements between the theoretical predictions and the results of ab initio calculations prove that the bonding theory is a powerful tool for the analysis of various boron materials. Now, let us explore the borophene nanoribbons with flat edges.

First, formation energies of triangular lattice-based ribbons with different widths, like single-, double-, and triple-chain, etc. (Figure 6a), are calculated using eq 1 and the result is shown in Figure 6b, denoted by black dots. It is shown that double-chain and triple-chain ribbons are energetically the most favorable ribbons. Further increasing the ribbon width leads to lower stability. The less stability of the wider triangular lattice-based ribbons is not a surprise because 2D borophene tends to form hexagonal holes to reduce the ratio of π electrons.^{8,14,20}

In the original study of the σ bond resonance theory,²⁰ we propose an occupation imbalance factor to measure the stability of borophene. The factor is defined as

$$\delta = N_e^\sigma / N_o^\sigma - N_e^\pi / N_o^\pi \quad (3)$$

where N_e^σ , N_o^σ , N_e^π , and N_o^π are the numbers of σ electrons, σ orbitals, π electrons, and π orbitals, respectively. δ is the electron-to-orbital ratio (N_e/N_o) difference between σ and π systems. If occupation ratios of the σ and π systems are the same or the occupations are balanced, $\delta = 0$. Numerous calculations showed that the occupation imbalance factor can be regarded as an indicator to measure the stability of flat boron materials. Smaller δ implies more stable borophene, and borophene isomers with $\delta = 0$ are the most stable ones.

To find the optimal δ for ribbons, we introduce hexagonal holes into wider ribbons to search for the most stable ribbon isomers (Figure 6a, see the caption of Figure S13 for details of the isomer generation). The optimized structures, the

calculated formation energies, and the corresponding occupation imbalance factor δ of these ribbons are presented in Figures S13–S16 and Tables S1–S4. As shown in Figure 6b, where the data for ribbons with holes are denoted by black circles, we can clearly see that introducing holes into the wide ribbons ($w > 5$) properly can reduce their formation energies or stabilize them. In Figure 6c, we plot the formation energies of various 5-, 6-, and 7-chain ribbons as a function of the imbalance factor, δ . A strong correlation between the formation energies and the imbalance factor is clearly shown. From the parabolic fitting of the low energy data, we can find that the most stable ribbon isomers always have imbalance factors close to 0.1, which is slightly different from $\delta = 0.0$ for 2D borophene.²⁰ This analysis clearly shows that the imbalance factor is an effective indicator of understanding the stability of borophene nanoribbons.

Double-Chain Protection of the Flat Edges

It is worth noting that there is a high kink in the energy curve in Figure 6b, which implies that the 4-chain ribbons are less stable than others. We search many isomers with different hexagonal hole patterns and δ values (Figure S9 and Table S1) and find that the 4-chain ribbons with holes are always less stable than the ribbons without holes. To understand the interesting phenomenon, we look into all of the ribbon isomers (5-, 6-, and 7-chain) with holes (Figures S14–S16). It can be seen that the most stable ribbon structures (denoted in black) never contain any hexagonal holes at the edges. Taking several 6-chain ribbons (Figure 7a,b) as examples, energies of the isomers with hexagonal holes exactly at the edge are mostly >2 eV/nm higher than those of the structures when the holes are moved one triangular lattice away from the edge. It has been reported that flat boron structures containing B atoms with a small coordination number (<4) are not energetically

favorable.¹⁴ The double-chain is like a special structure,^{9,17} which well protects the flat edge by avoiding the existence of the B atoms with small coordination numbers and therefore increases the stability.

We further analyzed the bonding configurations of the ribbon structures with and without hexagonal holes at the edge (Figure 7c–h). As presented in Figure 7e, when the hole appears at the ribbon edge and the hole edge coincides with the ribbon edge, the resonance of the ribbon edge interferes with that of the hole edge, and thus, both resonances break. In addition, at the edge of both the ribbon and hole, it shows particularly high electron density due to the coexistence of the unconventional 2c–2e bond of the ribbon edge and the conventional 2c–2e bond of the hole edge (highlighted by a red square, as shown in Figure 7e,f). In the case when both edges are well protected by the double-chain (Figure 7g,h), the resonances of both the ribbon edge and the hexagonal hole edge are reserved, and the VECD map also shows a good electron delocalization.

The above analysis indicates that double-chain protection is essential for the flat edge to be highly stable.¹⁷ We could therefore understand the energy kink at the 4-chain ribbons (Figure 6b). Although the introduction of hexagonal holes into the 4-chain ribbons can increase the occupation imbalance factor δ , approaching the optimized value, ~ 0.1 , it must break the double-chain protection of at least one edge (Figures 6b and S13) and, thus, the 4-chain ribbon appears a magic unstable structure among all ribbons.

We note that two preconditions of the double-chain protection mechanism are that the boron material is triangular lattice-based and the flat edge should be long enough. Small boron clusters containing largely deformed triangular lattices or short edges are beyond the scope of this study.

CONCLUSIONS

In summary, we have investigated the bonding configurations and stabilities of various borophene edges based on the theory of the σ bond resonance in sp^2 -hybridized boron materials. Different from the pristine edge of other 2D materials, the borophene edge can be self-terminated by adopting different bonding configurations at the edge to diminish the dangling bonds. Thus, the pristine borophene edges, especially the flat ones, own very high stability of ~ 2 – 3 eV/nm and can exist under ambient conditions. Such pristine edges can be used for different applications, such as catalysis and one-dimensional quantum materials. We further verify the analysis of bonding configurations of various boron edges by first-principle calculations. Based on the verified bonding theory, borophene nanoribbons with flat edges are further explored. Double-chain and triple-chain ribbons with triangular lattices are highly stable, and introducing a certain number of hexagonal holes in the central area of the ribbons is essential to stabilize the wider ribbons. The occupation imbalance factor, δ , which has been successfully applied to 2D borophene, is found to be an effective indicator to measure the stability of borophene nanoribbons. Moreover, we also show a double-chain protection mechanism of the borophene flat edge. This study reveals the origin of borophene's edge stability and proves that the bonding configuration theory can be used as a powerful tool for boron materials design.

METHODS

Details of the DFT calculations and the VECD maps. The planar boron nanoclusters and borophene nanoribbons were relaxed using DFT with Vienna ab initio Simulation Package (VASP).^{23,24} The projected augmented wave (PAW) method²⁵ and generalized gradient approximation (GGA)²⁶ energy for the exchange–correlation interactions were employed. The DFT-D3 method²⁷ was used to describe the weak van der Waals interaction (Figure S17), and the plane-wave cutoff energy was set as 400 eV. The Brillouin zone was sampled using Monkhorst–Pack k -mesh²⁸ with a separation criterion of 0.02. Criteria for energy and force convergence were 10^{-4} eV and 10^{-2} eV/Å in geometry optimization, and those were 10^{-5} eV and 10^{-2} eV/Å in the calculations of electronic properties, respectively. The criteria have been tested valid as shown in Figure S18 and Table S5. In all of the calculations, we turned on the spin with the parameter ISPIN = 2.

To calculate the formation energies of the free-standing borophene nanoribbons and nanoclusters, we used 3D supercells with all perpendicular (along the z -axis) and parallel (along the x -axis) vacuum distances larger than 15 Å. For the calculation of each ribbon or edge structure, the lattice constant along the ribbon length direction (y -axis) was optimized in advance.

To calculate the binding energy between borophene nanoribbons and a Ag substrate, the perpendicular vacuum distance (along the z -axis) was set larger than 12 Å, and a (111) three-layer Ag slab model with a fixed bottom layer was used to present the Ag(111) substrate. On the Ag(111) substrates, a minor strain ($<0.3\%$) was introduced into the ribbon (along the length direction, i.e., y -axis) because of the lattice mismatch between the borophene and fcc Ag(111) surface. In the supercell, the distances between the neighboring ribbons (along the x -axis) on the substrates were set larger than 10 Å to ensure that the interactions between neighboring slabs are negligible. Each ribbon was placed at several different positions of the substrates and the one with minimum energy was used for the final calculation and analysis.

ASSOCIATED CONTENT

Supporting Information

The Supporting Information is available free of charge at <https://pubs.acs.org/doi/10.1021/jacsau.3c00555>.

Additional calculation results, including the bonding analysis and VECD maps of various borophene ribbons and planar boron clusters; energies and detailed structures of various borophene ribbons (PDF)

AUTHOR INFORMATION

Corresponding Authors

Sung Youb Kim – Graduate School of Carbon Neutrality and Department of Mechanical Engineering, Ulsan National Institute of Science and Technology, Ulsan 44919, Republic of Korea; orcid.org/0000-0002-9417-4575; Email: sykim@unist.ac.kr

Feng Ding – Department of Materials Science and Engineering, Ulsan National Institute of Science and Technology, Ulsan 44919, Republic of Korea; Shenzhen Institute of Advanced Technology, Chinese Academy of Sciences, Shenzhen 518055, P.R. China; orcid.org/0000-0001-9153-9279; Email: gnding@gmail.com

Authors

Lu Qiu – Department of Materials Science and Engineering, Graduate School of Carbon Neutrality, and Department of Mechanical Engineering, Ulsan National Institute of Science and Technology, Ulsan 44919, Republic of Korea; orcid.org/0000-0001-8468-1904

Yuewen Mu – Key Laboratory of Materials for Energy Conversion and Storage of Shanxi Province and Institute of

Molecular Science, Shanxi University, Taiyuan 030006, P.R. China; orcid.org/0000-0002-0162-5091

Complete contact information is available at:
<https://pubs.acs.org/10.1021/jacsau.3c00555>

Author Contributions

F.D. supervised the project. L.Q. performed the calculations and bonding analysis. Y.M. conducted SSAdNDP calculation. L.Q. and F.D. analyzed the data and wrote the manuscript. All authors discussed the results and commented on the manuscript.

Notes

The authors declare no competing financial interest.

ACKNOWLEDGMENTS

L.Q. and S.Y.K. acknowledge the support from the Basic Research Laboratory Support Program (Grant No. 2021R1A4A1033224) of the National Research Foundation of Korea. F.D. acknowledges the support of the National Science Foundation of China (NSFC-22333005), High-Talent Support from the Shenzhen Institute of Advanced Technology (SIAT-SE3G0991010, 2023), and the Startup Research Grant from Shenzhen Institute of Advanced Technology.

REFERENCES

- (1) Zhai, H.-J.; Zhao, Y.-F.; Li, W.-L.; Chen, Q.; Bai, H.; Hu, H.-S.; Piazza, Z. A.; Tian, W.-J.; Lu, H.-G.; Wu, Y.-B.; Mu, Y.-W.; Wei, G.-F.; Liu, Z.-P.; Li, J.; Li, S.-D.; Wang, L.-S. Observation of an all-boron fullerene. *Nat. Chem.* **2014**, *6* (8), 727–731.
- (2) Mannix, A. J.; Zhou, X.-F.; Kiraly, B.; Wood, J. D.; Alducin, D.; Myers, B. D.; Liu, X.; Fisher, B. L.; Santiago, U.; Guest, J. R.; Yacaman, M. J.; Ponce, A.; Oganov, A. R.; Hersam, M. C.; Guisinger, N. P. Synthesis of borophenes: Anisotropic, two-dimensional boron polymorphs. *Science* **2015**, *350* (6267), 1513.
- (3) Feng, B.; Zhang, J.; Zhong, Q.; Li, W.; Li, S.; Li, H.; Cheng, P.; Meng, S.; Chen, L.; Wu, K. Experimental realization of two-dimensional boron sheets. *Nat. Chem.* **2016**, *8* (6), 563–568.
- (4) King, R. B. Three-Dimensional Aromaticity in Polyhedral Boranes and Related Molecules. *Chem. Rev.* **2001**, *101* (5), 1119–1152.
- (5) Eberhardt, W. H.; Crawford, B., Jr.; Lipscomb, W. N. The Valence Structure of the Boron Hydrides. *J. Chem. Phys.* **1954**, *22* (6), 989–1001.
- (6) Zhai, H.-J.; Alexandrova, A. N.; Birch, K. A.; Boldyrev, A. I.; Wang, L.-S. Hepta- and Octacoordinate Boron in Molecular Wheels of Eight- and Nine-Atom Boron Clusters: Observation and Confirmation. *Angew. Chem., Int. Ed.* **2003**, *42* (48), 6004–6008.
- (7) Piazza, Z. A.; Hu, H.-S.; Li, W.-L.; Zhao, Y.-F.; Li, J.; Wang, L.-S. Planar hexagonal B36 as a potential basis for extended single-atom layer boron sheets. *Nat. Commun.* **2014**, *5* (1), 3113.
- (8) Tang, H.; Ismail-Beigi, S. Novel Precursors for Boron Nanotubes: The Competition of Two-Center and Three-Center Bonding in Boron Sheets. *Phys. Rev. Lett.* **2007**, *99* (11), No. 115501.
- (9) Bai, H.; Chen, Q.; Miao, C.-Q.; Mu, Y.-W.; Wu, Y.-B.; Lu, H.-G.; Zhai, H.-J.; Li, S.-D. Ribbon aromaticity in double-chain planar BnH22- and Li2BnH2 nanoribbon clusters up to n = 22: lithiated boron dihydride analogues of polyenes. *Phys. Chem. Chem. Phys.* **2013**, *15* (43), 18872–18880.
- (10) Seenithurai, S.; Chai, J.-D. Electronic Properties of Linear and Cyclic Boron Nanoribbons from Thermally-Assisted-Occupation Density Functional Theory. *Sci. Rep.* **2019**, *9* (1), 12139.
- (11) Vishkayi, S. I.; Tagani, M. B. Edge-Dependent Electronic and Magnetic Characteristics of Freestanding β 12-Borophene Nanoribbons. *Nano-Micro Lett.* **2018**, *10* (1), 14.
- (12) Zhang, Z.; Penev, E. S.; Yakobson, B. I. Two-dimensional boron: structures, properties and applications. *Chem. Soc. Rev.* **2017**, *46* (22), 6746–6763.
- (13) Penev, E. S.; Bhowmick, S.; Sadzadeh, A.; Yakobson, B. I. Polymorphism of Two-Dimensional Boron. *Nano Lett.* **2012**, *12* (5), 2441–2445.
- (14) Wang, Y.; Park, Y.; Qiu, L.; Mitchell, I.; Ding, F. Borophene with Large Holes. *J. Phys. Chem. Lett.* **2020**, *11* (15), 6235–6241.
- (15) Liu, Y.; Dobrinsky, A.; Yakobson, B. I. Graphene Edge from Armchair to Zigzag: The Origins of Nanotube Chirality? *Phys. Rev. Lett.* **2010**, *105* (23), No. 235502.
- (16) Vorontsov, A. V.; Tretyakov, E. V. Determination of graphene's edge energy using hexagonal graphene quantum dots and PM7 method. *Phys. Chem. Chem. Phys.* **2018**, *20* (21), 14740–14752.
- (17) Zhang, Z.; Mannix, A. J.; Liu, X.; Hu, Z.; Guisinger, N. P.; Hersam, M. C.; Yakobson, B. I. Near-equilibrium growth from borophene edges on silver. *Science Advances* **2019**, *5* (9), No. eaax0246.
- (18) Zubarev, D. Y.; Boldyrev, A. I. Comprehensive analysis of chemical bonding in boron clusters. *J. Comput. Chem.* **2007**, *28* (1), 251–268.
- (19) King, R. B. Planar Networks of Boron Triangles: Analogies to Benzene and Other Planar Aromatic Hydrocarbons. *J. Phys. Chem. A* **2022**, *126* (6), 901–909.
- (20) Qiu, L.; Zhang, X.; Kong, X.; Mitchell, I.; Yan, T.; Kim, S. Y.; Yakobson, B.; Ding, F. Theory of sigma bond resonance in flat boron materials. *Nat. Commun.* **2023**, *14* (1), 1804.
- (21) Galeev, T. R.; Dunnington, B. D.; Schmidt, J. R.; Boldyrev, A. I. Solid state adaptive natural density partitioning: a tool for deciphering multi-center bonding in periodic systems. *Phys. Chem. Chem. Phys.* **2013**, *15*, S022–S029.
- (22) Koskinen, P.; Malola, S.; Häkkinen, H. Self-Passivating Edge Reconstructions of Graphene. *Phys. Rev. Lett.* **2008**, *101* (11), No. 115502.
- (23) Kresse, G.; Hafner, J. Ab initio molecular dynamics for open-shell transition metals. *Phys. Rev. B* **1993**, *48* (17), 13115–13118.
- (24) Kresse, G.; Furthmüller, J. Efficiency of ab-initio total energy calculations for metals and semiconductors using a plane-wave basis set. *Comput. Mater. Sci.* **1996**, *6* (1), 15–50.
- (25) Kresse, G.; Joubert, D. From ultrasoft pseudopotentials to the projector augmented-wave method. *Phys. Rev. B* **1999**, *59* (3), 1758–1775.
- (26) Perdew, J. P.; Burke, K.; Ernzerhof, M. Generalized Gradient Approximation Made Simple. *Phys. Rev. Lett.* **1996**, *77* (18), 3865–3868.
- (27) Grimme, S.; Antony, J.; Ehrlich, S.; Krieg, H. A consistent and accurate ab initio parametrization of density functional dispersion correction (DFT-D) for the 94 elements H-Pu. *J. Chem. Phys.* **2010**, *132* (15), 154104.
- (28) Monkhorst, H. J.; Pack, J. D. Special points for Brillouin-zone integrations. *Phys. Rev. B* **1976**, *13* (12), 5188–5192.